Transverse energy-energy correlator for vector boson-tagged hadron production in *pp* and *pA* collisions

Zhong-Bo Kang,[1,2,3,*] Sookhyun Lee,[4,5,†] Jani Penttala,[1,2,‡] Fanyi Zhao,[6,§] and Yiyu Zhou[7,8,9,1,‖]

[1]*Department of Physics and Astronomy, University of California, Los Angeles, California 90095, USA*
[2]*Mani L. Bhaumik Institute for Theoretical Physics, University of California, Los Angeles, California 90095, USA*
[3]*Center for Frontiers in Nuclear Science, Stony Brook University, Stony Brook, New York 11794, USA*
[4]*Physics Department, University of Tennessee, Knoxville, Tennessee 37996, USA*
[5]*Physics Department, University of Michigan, Ann Arbor, Michigan 48109, USA*
[6]*Center for Theoretical Physics, Massachusetts Institute of Technology, Cambridge, Massachusetts 02139, USA*
[7]*Department of Physics, University of Turin, via Pietro Giuria 1, I-10125 Torino, Italy*
[8]*Key Laboratory of Atomic and Subatomic Structure and Quantum Control (MOE), Guangdong Basic Research Center of Excellence for Structure and Fundamental Interactions of Matter, Institute of Quantum Matter, South China Normal University, Guangzhou 510006, China*
[9]*Guangdong-Hong Kong Joint Laboratory of Quantum Matter, Guangdong Provincial Key Laboratory of Nuclear Science, Southern Nuclear Science Computing Center, South China Normal University, Guangzhou 510006, China*

(Received 11 October 2024; accepted 9 June 2025; published 7 July 2025)

We investigate the transverse energy-energy correlator (TEEC) event-shape observable for back-to-back $\gamma + h$ and $Z + h$ production in both pp and pA collisions. Our study incorporates nuclear modifications into the transverse-momentum dependent (TMD) factorization framework, with resummation up to next-to-leading logarithmic accuracy, for TEEC as a function of the variable $\tau = (1 + \cos\phi)/2$, where ϕ is the azimuthal angle between the vector boson and the final hadron. We analyze the nuclear modification factor R_{pA} in pAu collisions at Relativistic Heavy Ion Collider and pPb collisions at the Large Hadron Collider. Our results demonstrate that the TEEC observable is a sensitive probe for nuclear modifications in TMD physics. Specifically, the changes in the τ-distribution shape provide insights into transverse momentum broadening effects in large nuclei, while measurements at different rapidities allow us to explore nuclear modifications in the collinear component of the TMD parton distribution functions in nuclei.

DOI: 10.1103/1djw-8zrh

I. INTRODUCTION

Event-shape observables are inherently sensitive to various energy scales anywhere between the hard scale and the nonperturbative scale of quantum chromodynamics (QCD). Along with the collision system and the entities of choice that define an event-shape observable, how we define the observable can magnify particular aspects of the event topology, allowing us to zoom in on the underlying physics of interest. At e^+e^- and ep colliders, event shapes traditionally have played a crucial role in determining the strong coupling constant α_s [1–3]. At the Large Hadron Collider (LHC), event-shape observables suitable for pp collisions have also been introduced [4] and, in particular, observables that use jets as inputs in multijet events have been extensively measured in the past decade [5–12]. These observables are known for their high precision in theory calculations [13,14]. Recently, observables that define their shapes in terms of particles inside jets rather than jets themselves are often measured [15–19]. Such observables provide enhanced sensitivities to collinear and soft emissions. For this reason, their measurements allow for in-depth studies of radiation patterns and nonperturbative effects and are used to fine-tune parton shower and hadronization models in Monte Carlo simulations. Furthermore, fully global event shapes [20–22] have been computed with a state-of-the-art theoretical precision for deep inelastic scattering (DIS), where an experimentally clean

*Contact author: zkang@physics.ucla.edu
†Contact author: shlee@bnl.gov
‡Contact author: janipenttala@physics.ucla.edu
§Contact author: fanyi@mit.edu
‖Contact author: yiyu.zhou@unito.it

Published by the American Physical Society under the terms of the Creative Commons Attribution 4.0 International license. Further distribution of this work must maintain attribution to the author(s) and the published article's title, journal citation, and DOI. Funded by SCOAP³.

environment is advantageous in achieving xhigh-precision measurements. These types of observables are gaining increasing attention due to their potentially greater handle on nonperturbative QCD power corrections. Some have been measured recently [23,24], and theoretical development is ongoing for measurements planned at the future Electron-Ion Collider [25–28]. Additionally, event-shape observables are great tools for discovering new physics phenomena, e.g., constraining new colored matter [29,30].

In this paper, we will focus in particular on the transverse energy-energy correlator (TEEC) event-shape observable. TEEC [31] is an extension of the energy-energy correlator (EEC) [32,33], which was initially introduced for e^+e^- collisions to characterize global event shapes, and has been broadly investigated at different experiments [34–47]. Later on, TEEC was defined such that it incorporates the transverse energy of the hadrons and is a more suitable observable for hadronic collider environments [9,10,48–50]. Recently, TEEC has been computed for lepton-hadron production in lepton-proton scattering [51,52]. At the LHC, the EEC has also been measured using particles inside jets [53,54].

A great advantage of the EEC and TEEC observables over other event-shape observables is that they effectively suppress contributions from soft radiation of low-energy nature and therefore become less sensitive to hadronization effects. Another advantage of the TEEC lies in the accurate reconstruction of collision kinematics in the laboratory frame as highlighted in Ref. [55]. In the back-to-back limit of the EEC and TEEC, results can be written directly in terms of the transverse-momentum dependent (TMD) parton distribution functions, enabling highly accurate predictions upon the resummation of Sudakov logarithms. All of these make the TEEC a unique lens through which to investigate the transverse-momentum dependent structures of the proton [51,56] and advance our understanding of nonperturbative dynamics of QCD.

Measuring hadrons in jets recoiling against a vector boson, Z or γ, allows us to focus on a certain parton flavor as has been exploited in studying jet fragmentation properties in pp collisions [57–60]. Utilizing all hadrons in the back-to-back limit of this process when measuring the TEEC observable provides a clean access to the gluon TMD and the nonperturbative component of the light-quark TMD fragmentation function (FF). Experimentally, low-energy hadrons are challenging to measure because of a high level of background consisting of spurious particles and large measurement uncertainties. The TEEC observables are defined in such a way that they naturally suppress soft particles, reducing the sensitivity to the low-energy background. In addition, the absence of the jet radius parameter and collinear-soft functions simplifies theoretical computations. The TEEC for γ/Z-jet production in hadron colliders has been recently studied in [61] at next-to-next-to-next-to-leading logarithmic ($\mathrm{N^3LL}$) accuracy.

Another aspect of this process that can be explored is its sensitivity to the nuclear medium [62–68]. As the vector boson does not experience strong interaction, its momentum is not modified by the medium. This enables us to quantify the transverse momentum of the parton produced in the initial-state scattering. The jet, on the other hand, loses its energy through interactions with the medium. Measuring how much energy is lost leads us to gain insights into the role that nuclear medium plays in altering the initial partonic dynamics inside the proton. The nuclear modification of this kind has been observed in measurements of the dijet and photon-jet momentum imbalance [69–72], along with jet fragmentation functions [73,74]. It is therefore of great interest to study if similar effects can be found for the TEEC between vector bosons and hadrons.

The rest of the paper is organized as follows. In Sec. II, we present the theoretical formalism for the TEEC in pp to boson-hadron production. With the factorization at hand, all the ingredients appearing in the factorization formula are discussed. They include the hard function, TMD parton distribution functions (PDFs), TEEC jet functions and soft function. Additionally, we provide the TMD PDFs and TEEC jet functions in a nucleus that are needed to study nuclear modification for the TEEC in pA collisions. In Sec. III, we explore phenomenological impact of the TEEC as a potential probe into these nuclear TMD PDFs and TEEC jet functions at both relativistic heavy ion collider (RHIC) and LHC kinematics. Finally, we summarize our work in Sec. IV.

II. THEORETICAL FORMALISM

In this section, we outline the factorization of the transverse energy-energy correlation between a vector boson and final-state hadrons in the back-to-back limit. The process is illustrated in Fig. 1 and is given as,

$$p(P_A) + p(P_B) \to V(p_V) + h(p_h) + X, \tag{1}$$

where p, V and h denote the initial-state proton, final-state vector boson (either photon or Z-boson) and final-state hadron. The momentum of each particle is given in parenthesis. With $E_{T,V}$ and $E_{T,h}$ denoting the transverse energy of the vector boson V and the final-state hadron h, we define the TEEC as,

$$\begin{aligned}\mathbf{TEEC} &= \sum_h \int \mathrm{d}\sigma \frac{E_{T,V}E_{T,h}}{E_{T,V}\sum_{h'} E_{T,h'}} \delta\left(\tau - \frac{1+\cos\phi}{2}\right) \\ &= \sum_h \int \mathrm{d}\sigma \frac{E_{T,h}}{\sum_{h'} E_{T,h'}} \delta\left(\tau - \frac{1+\cos\phi}{2}\right).\end{aligned} \tag{2}$$

In this definition, the contributions from all the final-state hadrons are summed over. The variable τ is defined by $\tau \equiv (1+\cos\phi)/2$, where ϕ is the azimuthal angle between the vector boson and hadron h in the xy-plane as illustrated

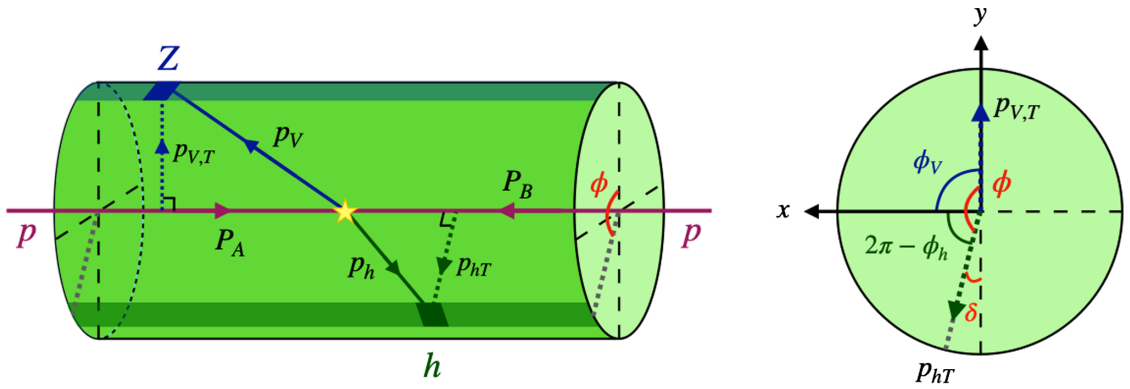


FIG. 1. Left: Illustration of TEEC in the pp center-of-mass frame. The incoming proton momentum P_A and P_B define the z axis. The transverse momentum of the outgoing vector boson $\boldsymbol{p}_{V,T}$ defines the $+y$ direction and hence the xy-plane is determined. Right: The xy-plane of the left panel.

in Fig. 1. One can easily find that in the back-to-back configuration where ϕ approaches π, $\pi - \phi = \pi - (2\pi - \phi_h + \phi_V) = \phi_h - \phi_V - \pi$ is a small angle, and $\tau \ll 1$.

The factorization formalism of the TEEC as defined in Eq. (2) is then expressed as,

$$\begin{aligned}\frac{\mathrm{d}\Sigma}{\mathrm{d}\tau \mathrm{d}y_V \mathrm{d}p_{V,T}} &= \sum_{a,b,c} \frac{p_{V,T}}{\sqrt{\tau}} \int_{-\infty}^{\infty} \frac{\mathrm{d}b}{2\pi} e^{-2ib\sqrt{\tau}p_{V,T}} \int \mathrm{d}y_c H_{ab\to Vc}(y_V, p_{V,T}, m_V, \mu) \\ &\quad \times x_a f_{1,a/p}^{(u)}\left(x_a, b, \mu, \frac{\zeta_a}{\nu^2}\right) x_b f_{1,b/p}^{(u)}\left(x_b, b, \mu, \frac{\zeta_b}{\nu^2}\right) J_c^{(u)}\left(b, \mu, \frac{\zeta_c}{\nu^2}\right) S_{abc}(b, \mu, \nu) \\ &= \sum_{a,b,c} \frac{p_{V,T}}{\sqrt{\tau}} \int_{0}^{\infty} \frac{\mathrm{d}b}{\pi} \cos(2b\sqrt{\tau}p_{V,T}) \int \mathrm{d}y_c H_{ab\to Vc}(y_V, p_{V,T}, m_V, \mu) \\ &\quad \times x_a f_{1,a/p}^{(u)}\left(x_a, b, \mu, \frac{\zeta_a}{\nu^2}\right) x_b f_{1,b/p}^{(u)}\left(x_b, b, \mu, \frac{\zeta_b}{\nu^2}\right) J_c^{(u)}\left(b, \mu, \frac{\zeta_c}{\nu^2}\right) S_{abc}(b, \mu, \nu), \end{aligned} \tag{3}$$

where y_V and $p_{V,T}$ denote the rapidity and transverse momentum of the vector boson, respectively. The subscripts a, b and c in $H_{ab\to Vc}$ can take a parton species, q for a quark, $\bar{q}$ for an antiquark, and g for a gluon. Here y_c is the rapidity of the parton c that initiates the TEEC jet J_c, and m_V is the mass of the produced vector boson. The y_c dependence is implicit and will be detailed in Sec. II A.

Since the momentum imbalance is along the x axis by definition, we have $\boldsymbol{b} \equiv (b_x, b_y) = (b, 0)$. As a result, the dimensionality of the Fourier transform becomes 1 as previously pointed out in, e.g., [51,75,76]. In the factorization formalism, $f_{1,i/p}^{(u)}(x_i, b, \mu, \zeta_i/\nu^2)$ for parton species i is its "unsubtracted" TMD PDF, where x_i is the collinear momentum fraction of the parent hadron carried by parton i and ζ_i is the Collins-Soper parameter. It is worth noting that b contains only the x component as discussed above. The "unsubtracted" TMD PDFs describe energetic radiations of incoming partons in the direction collinear to the incoming protons [77].

The hard function $H_{ab\to Vc}(y_V, p_{V,T}, m_V, \mu)$ contains the virtual corrections to the underlying partonic process $ab \to Vc$ that can be obtained through matching calculations between QCD and the soft-collinear effective theory. The wide-angle soft emissions connecting initial and final colored particles abc are encoded in the soft function $S_{abc}(b, \mu, \nu)$. Finally, $J_c^{(u)}(b, \mu, \zeta_c/\nu^2)$ is the "unsubtracted" TEEC jet function, which has a close relation with the TMD fragmentation functions, and will be discussed in Sec. II C. To arrive at the last line of Eq. (3), we exploited the fact that $f_{1,i/p}^{(u)}$, S_{abc} and $J_c^{(u)}$ are all even functions of b (they all depend on b^2). The TMD PDFs, soft function and TEEC jet function also depend on the renormalization scale μ and the rapidity renormalization scale ν [78]. Furthermore, $\zeta_{a,b,c}$ in TMD PDFs or TEEC jet function are the Collins-Soper parameters and will be discussed in Sec. II A and II C.

In the rest of this section, we will quantitatively define and discuss in detail each ingredient in the factorization formula in Eq. (3).

A. Hard function and TMD PDFs

In Eq. (3), $H_{ab\to Vc}(y_V, p_{V,T}, \mu)$ is the hard function that describes the partonic scattering process $ab \to Vc$. The

hard function $H_{ab\to Vc}$ at LO is given as [79,80],

$$H^{(0)}_{q\bar{q}\to Vg} = \frac{\mathcal{N}_H(N_c^2-1)}{N_c^2}\frac{\hat{t}^2+\hat{u}^2+2\hat{s}m_V^2}{\hat{t}\,\hat{u}}, \tag{4}$$

$$H^{(0)}_{qg\to Vq} = -\frac{\mathcal{N}_H}{N_c}\frac{\hat{s}^2+\hat{t}^2+2\hat{u}m_V^2}{\hat{s}\,\hat{t}}, \tag{5}$$

where N_c is the number of colors for quarks and the normalization $\mathcal{N}_H$ given by,

$$\mathcal{N}_H \equiv \frac{2\pi p_{V,T}}{\hat{s}^2}\alpha_s\alpha_{\rm em}\alpha_q. \tag{6}$$

The mass of vector boson m_V for photons is set to 0, i.e., $m_\gamma = 0$ GeV, while for the Z boson m_Z is set at 91.1876 GeV. The fine structure constants $\alpha_{\rm em}$ used in phenomenological studies are $1/137$ and $1/128$ for $V=\gamma$ and $V=Z$, respectively, and α_s is the strong coupling constant. The parameter α_q for $\gamma+h$ production is,

$$\alpha_q \equiv e_q^2, \tag{7}$$

where e_q denotes the electric charge of the quark. For $Z+h$ production, α_q is given by,

$$\alpha_q \equiv \frac{1-4|e_q|\sin^2(\theta_W)+8e_q^2\sin^4(\theta_W)}{8\sin^2(\theta_W)\cos^2(\theta_W)}, \tag{8}$$

where $\cos\theta_W = 0.88168$. The collinear momentum fractions x_a and x_b are given by,

$$x_a = \frac{1}{\sqrt{s}}\left(\sqrt{p_{V,T}^2+m_V^2}e^{y_V}+p_{V,T}e^{y_c}\right), \tag{9}$$

$$x_b = \frac{1}{\sqrt{s}}\left(\sqrt{p_{V,T}^2+m_V^2}e^{-y_V}+p_{V,T}e^{-y_c}\right), \tag{10}$$

where $\sqrt{s}$ is the center-of-mass energy for the collision. Finally, $\hat{s}$, $\hat{t}$ and $\hat{u}$ appearing in Eqs. (4) and (5) are the partonic Mandelstam variables. To define them, we first list the three relevant partonic processes:

$$q(p_a)+\bar{q}(p_b)\to V(p_V)+g(p_c), \tag{11}$$

$$q(p_a)+g(p_b)\to V(p_V)+q(p_c), \tag{12}$$

$$\bar{q}(p_a)+g(p_b)\to V(p_V)+\bar{q}(p_c), \tag{13}$$

where q, $\bar{q}$ and g denote quark, antiquark and gluon, respectively, and V denotes the vector boson. The partonic Mandelstam variables are then defined as,

$$\hat{s}\equiv(p_a+p_b)^2, \quad \hat{t}\equiv(p_a-p_V)^2, \quad \hat{u}\equiv(p_b-p_V)^2. \tag{14}$$

The next-to-leading order (NLO) hard function used in this paper is given in [80]. Writing down the next-to-leading logarithmic NLL resummation requires the hard anomalous dimension up to one-loop order [79,81],

$$\gamma_\mu^H(\alpha_s) = -\sum_{i=a,b,c}\gamma_i[\alpha_s(\mu)] + \Gamma_{\rm cusp}[\alpha_s(\mu)]\left[C_a\ln\left(\frac{\hat{u}^2}{p_{V,T}^2\mu^2}\right)+C_b\ln\left(\frac{\hat{t}^2}{p_{V,T}^2\mu^2}\right)+C_c\ln\left(\frac{p_{V,T}^2}{\mu^2}\right)\right]+\mathcal{O}(\alpha_s^2), \tag{15}$$

where the cusp anomalous dimensions $\Gamma_{\rm cusp}$ and noncusp anomalous dimensions γ_i are expanded as,

$$\Gamma_{\rm cusp}[\alpha_s(\mu)] = \sum_{n=1}\Gamma_{n-1}\left(\frac{\alpha_s}{4\pi}\right)^n, \tag{16}$$

$$\gamma_i[\alpha_s(\mu)] = \sum_{n=1}\gamma_{n-1}^i\left(\frac{\alpha_s}{4\pi}\right)^n. \tag{17}$$

For the expansion we keep the following terms [82–84]:

$$\Gamma_0 = 4, \qquad \gamma_0^q = 6C_F, \qquad \gamma_0^g = 2\beta_0, \tag{18}$$

$$\Gamma_1 = C_A\left(\frac{268}{9}-\frac{4\pi^2}{3}\right)-\frac{80}{9}T_F n_f, \tag{19}$$

where $C_F = 4/3$, $C_A = 3$, $T_F = 1/2$ and n_f is the number of flavors. And β_0 is defined as,

$$\beta_0 \equiv \frac{11}{3}C_A - \frac{4}{3}T_F n_f. \tag{20}$$

Next, we provide a brief overview of the TMD PDFs $f^{(u)}_{1,i/p}(x_i,b,\mu,\zeta_i/\nu^2)$ for an incoming parton i. As discussed in [52], two scales other than μ are involved in the "unsubtracted" TMD PDFs $f^{(u)}_{1,i/p}(x_i,b,\mu,\zeta_i/\nu^2)$: the Collins-Soper scale ζ [77,85,86] and the rapidity renormalization scale ν [78]. For both quark and gluon TMD PDFs $f^{(u)}_{1,i/p}$, the rapidity divergences can be canceled by subtracting the square root of the standard soft function $S_{n_i\cdot\bar{n}_i}(b,L,L_\nu)$. Denoted by n_i is the lightlike directional four-vector of an incoming or outgoing parton moving with a momentum p_i defined in Eqs. (11) to (13), and L and L_ν will be defined in Eq. (21). Adopting dimensional regularization in $4-2\epsilon$ space-time dimensions and the rapidity regulator η discussed in [78], the standard soft function is given by [85,87],

$$S_{n_i\cdot\bar{n}_i}(b,L,L_\nu) = 1 - \frac{\alpha_s C_i}{2\pi}\left[2\left(\frac{2}{\eta}+L_\nu\right)\left(\frac{1}{\epsilon}+L\right) - \frac{2}{\epsilon^2}+L^2+\frac{\pi^2}{6}\right], \tag{21}$$

where $L \equiv \ln(\mu^2/\mu_b^2)$ with $\mu_b \equiv 2e^{-\gamma_E}/b$, $L_\nu \equiv \ln(\nu^2/\mu^2)$, C_i takes the value of C_F or C_A for quark and gluon TMD PDFs, respectively, and γ_E is the Euler-Mascheroni constant. Using $S_{n_i\cdot\bar{n}_i}$ from Eq. (21), we additionally define the "subtracted" parton distribution $f_{1,i/p}(x_i,b,\mu,\zeta_i)$ that is free from the rapidity divergence [85],

$$f_{1,i/p}(x_i,b,\mu,\zeta_i) = f^{(u)}_{1,i/p}\left(x_i,b,\mu,\frac{\zeta_i}{\nu^2}\right) \times \sqrt{S_{n_i\cdot\bar{n}_i}(b,L,L_\nu)}. \tag{22}$$

The TMD evolution for the "subtracted" TMD PDFs is now given by the Collins-Soper evolution and the renormalization group equation, each associated with the Collins-Soper scale ζ [77,85] and the scale μ, respectively. The evolution equations are given by,

$$\frac{\mathrm{d}}{\mathrm{d}\ln\sqrt{\zeta}}\ln f_{1,i/p}(x_i,b,\mu,\zeta) = K(b,\mu), \tag{23}$$

$$\frac{\mathrm{d}}{\mathrm{d}\ln\mu}\ln f_{1,i/p}(x_i,b,\mu,\zeta_i) = \gamma^f_{\mu,i}\left[\alpha_s(\mu),\frac{\zeta_i}{\mu^2},\right] \tag{24}$$

where $K(b,\mu)$ denotes the Collins-Soper evolution kernel [77,85,88,89], and $\gamma^f_{\mu,i}[\alpha_s(\mu),\zeta_i/\mu^2]$ is the μ evolution kernel that evolves $f_{1,i/p}(x_i,b,\mu,\zeta_i)$ in scale μ at fixed $\zeta=\zeta_i$. Up to two-loop order, $\gamma^f_{\mu,i}$ is given by,

$$\gamma^f_{\mu,i}\left[\alpha_s(\mu),\frac{\zeta_i}{\mu^2}\right] = -C_i\Gamma_{\mathrm{cusp}}[\alpha_s(\mu)]\ln\left(\frac{\zeta_i}{\mu^2}\right)+\gamma_i[\alpha_s(\mu)], \tag{25}$$

where $C_i = C_F$ (C_A) for $i=q$ (g), and Γ_{cusp} and γ_i are the cusp and noncusp anomalous dimensions, respectively. They are given in Eqs. (16) and (17).

Solving the renormalization group equations on ζ and μ while taking into account the nonperturbative contributions from the large $b \gg 1/\Lambda_{\mathrm{QCD}}$ region, we obtain the expressions for TMD PDFs,

$$f_{1,i/p}(x_i,b,\mu,\zeta_i) = f_{1,i/p}(x_i,b,\mu_{b_*},\mu^2_{b_*}) \times \exp[-S^i_{\mathrm{NP}}(b,Q_0,\zeta_i)] \times \exp[-S^i_{\mathrm{pert}}(\mu,\mu_{b_*},\zeta_i)], \tag{26}$$

where we evolve the TMD PDFs from initial scales (μ_0,ζ_0) to final scales $(\mu,\zeta_i=\hat{s})$. We have chosen the following initial scales $\mu_0=\sqrt{\zeta_0}=\mu_{b_*}$. As usual, we define $\mu_{b_*} \equiv 2e^{-\gamma_E}/b_*$ and $b_* \equiv b/\sqrt{1+b^2/b^2_{\mathrm{max}}}$ with $b_{\mathrm{max}} = 1.5\ \mathrm{GeV}^{-1}$ following the b_* prescription [90–93]. The choice of $\zeta_i=\hat{s}$ for the incoming partons will be discussed in Sec. II C. The perturbative Sudakov factor $S^i_{\mathrm{pert}}(\mu,\mu_{b_*},\zeta_i)$ is given by,

$$S^i_{\mathrm{pert}}(\mu,\mu_{b_*},\zeta_i) = -K(b_*,\mu_{b_*})\ln\left(\frac{\sqrt{\zeta_i}}{\mu_{b_*}}\right) - \int_{\mu_{b_*}}^{\mu}\frac{\mathrm{d}\mu'}{\mu'}\gamma^f_{\mu,i}\left[\alpha_s(\mu'),\frac{\zeta_i}{\mu'^2}\right], \tag{27}$$

and the nonperturbative Sudakov factor for $i=q$ is given by [90,91],

$$S^i_{\mathrm{NP}}(b,Q_0,\zeta_i) = \frac{g_2}{2}\ln\left(\frac{b}{b_*}\right)\ln\left(\frac{\sqrt{\zeta_i}}{Q_0}\right)+g^q_1 b^2, \tag{28}$$

with $Q_0^2 = 2.4\ \mathrm{GeV}^2$, $g_2 = 0.84$ and $g^q_1 = 0.106\ \mathrm{GeV}^2$. For $i=g$, we will follow [94–96] and adopt the following parametrization:

$$S^i_{\mathrm{NP}}(b,Q_0,\zeta_i) = \frac{C_A}{C_F}\frac{g_2}{2}\ln\left(\frac{b}{b_*}\right)\ln\left(\frac{\sqrt{\zeta_i}}{Q_0}\right)+g^q_1 b^2, \tag{29}$$

where we set $g^q_1 = g^q_1$. Throughout this paper, we work at the next-to-leading logarithmic (NLL) level in resummation accuracy, where $K(b_*,\mu_{b_*})=0$.

In the conventional TMD approach [77], one can express $f_{1,i/p}(x,b,\mu_{b_*},\mu^2_{b_*})$ in terms of the collinear parton distribution functions through operator product expansion

$$f_{1,i/p}(x_i,\mu_{b_*}) = \sum_j\int_{x_i}^1\frac{\mathrm{d}x'}{x'}C_{i\leftarrow j}\left(\frac{x_i}{x'},\mu_{b_*}\right)f_{j/p}(x',\mu_{b_*}) \equiv [C_{i\leftarrow j}\otimes f_{j/p}](x_i,\mu_{b_*}), \tag{30}$$

where we adopt a shorthand notation $f_{1,i/p}(x_i,\mu_{b_*})$ for TMD PDFs and $f_{j/p}(x,\mu)$ denotes the proton collinear parton distribution of flavor j. The matching coefficients $C_{i\leftarrow j}$ are perturbatively calculable and can be found in, e.g., [85,90,97–102].

The nuclear modification is considered by substituting the nuclear collinear PDFs $f_{j/A}$ for the vacuum collinear PDFs $f_{j/p}$ in Eq. (30). In this work we adopt the EPPS16 set [103] for both gold (Au) and lead (Pb). For the proton PDFs, we use CT14nlo [104] to be consistent with the choice made in EPPS16. Additionally, we follow the work in [105] and introduce a modified nonperturbative parameter $g^q_{1,A}$ in place of g^q_1 in Eq. (28),

$$g^q_{1,A} = g^q_1 + a_N L, \tag{31}$$

where $L \equiv A^{1/3} - 1$ with A being the mass number of the nucleus. Our choice of nuclear broadening parameter $a_N = 0.016\ \mathrm{GeV}^2$ was determined in [105] from fitting experimental data using EPPS16 set [103] as the collinear baseline. The parameters a_N, as well as b_N, which will be discussed later in Sec. II C, are fitted from the semi-inclusive deep inelastic scattering (SIDIS) in electron-nucleus collisions and Drell-Yan (DY) dilepton production in proton-nucleus collisions [105]. Although the universality of these parameters across SIDIS, DY and TEEC observables remains an assumption, future measurements of TEEC and other TMD observables will ultimately assess its validity.

B. Soft function

The soft function for $V + h$ production can be computed with the rapidity regulator [106], and the expressions are given by [51,52,75,107],

$$\begin{aligned} S_{abc}(b,\mu,\nu) = 1 &- \boldsymbol{T}_a \cdot \boldsymbol{T}_b S^{(1)}_{n\cdot\bar{n}}(b, L, L_\nu + \ln(n_{ab})) \\ &- \boldsymbol{T}_b \cdot \boldsymbol{T}_c S^{(1)}_{n\cdot\bar{n}}(b, L, L_\nu + \ln(n_{bc})) \\ &- \boldsymbol{T}_c \cdot \boldsymbol{T}_a S^{(1)}_{n\cdot\bar{n}}(b, L, L_\nu + \ln(n_{ca})), \end{aligned} \tag{32}$$

where $\boldsymbol{T}_{a,b,c}$ are color factors, and $S^{(1)}_{n\cdot\bar{n}}$ is the NLO component defined by the relation $S_{n_i\cdot\bar{n}_i} = 1 + C_i S^{(1)}_{n\cdot\bar{n}}$ for the standard soft function given in Eq. (21). We have also defined $n_{ab} \equiv n_a \cdot n_b/2$.

Using color conservation $\boldsymbol{T}_a + \boldsymbol{T}_b + \boldsymbol{T}_c = 0$, we obtain,

$$\begin{aligned} S_{abc}(b,\mu,\nu) = 1 &+ \frac{1}{2}(\boldsymbol{T}_a^2 + \boldsymbol{T}_b^2 + \boldsymbol{T}_c^2) S^{(1)}_{n\cdot\bar{n}}(b, L, L_\nu) \\ &- \frac{\alpha_s L}{2\pi} \sum_{\mathrm{cyc}} (\boldsymbol{T}_a^2 + \boldsymbol{T}_b^2 - \boldsymbol{T}_c^2) \ln(n_{ab}) \\ &- \frac{\alpha_s L}{2\pi} \frac{1}{\epsilon} \sum_{\mathrm{cyc}} (\boldsymbol{T}_a^2 + \boldsymbol{T}_b^2 - \boldsymbol{T}_c^2) \ln(n_{ab}), \end{aligned} \tag{33}$$

where $\boldsymbol{T}^2_{q(g)} = C_F\ (C_A)$ and $\sum_{\mathrm{cyc}}$ represents a cyclic summation over the indices a, b and c.

Next we define the so-called "proper" TMD global soft function which does not depend on the rapidity scale ν,

$$S^{g,\mathrm{bare}}_{abc}(b,\mu) = \frac{1}{\sqrt{S_{n_a\cdot\bar{n}_a} S_{n_b\cdot\bar{n}_b} S_{n_c\cdot\bar{n}_c}}} S_{abc}(b,\mu,\nu). \tag{34}$$

The renormalized TMD global soft function $S^g_{abc}(b,\mu)$ is,

$$S^g_{abc}(b,\mu) = 1 - \frac{\alpha_s L}{2\pi} \sum_{\mathrm{cyc}} (\boldsymbol{T}_a^2 + \boldsymbol{T}_b^2 - \boldsymbol{T}_c^2) \ln(n_{ab}). \tag{35}$$

The renormalization group equation for S^g_{abc} is given as,

$$\frac{\mathrm{d}}{\mathrm{d}\ln\mu} \ln S^g_{abc}(b,\mu) = \gamma^S_\mu(\alpha_s), \tag{36}$$

where the anomalous dimension γ^S_μ is given by,

$$\gamma^S_\mu(\alpha_s) = -\frac{\alpha_s}{\pi} \sum_{\mathrm{cyc}} (\boldsymbol{T}_a^2 + \boldsymbol{T}_b^2 - \boldsymbol{T}_c^2) \ln(n_{ab}). \tag{37}$$

One can work out the scalar products n_{ab} in the above equation [61],

$$n_{ab} = 1, \qquad n_{ac} = \frac{-\hat{u}}{\hat{s} - m_V^2}, \qquad n_{bc} = \frac{-\hat{t}}{\hat{s} - m_V^2}, \tag{38}$$

where the partonic Mandelstam variables $\hat{s}$, $\hat{t}$ and $\hat{u}$ are given in Eq. (14).

C. TEEC jet function

We have introduced the "unsubtracted" TEEC jet function $J^{(u)}_c(b,\mu,\zeta_c/\nu^2)$ in Eq. (3). Its relation to the "unsubtracted" transverse momentum dependent fragmentation functions (TMD FFs) is given by [108],

$$J^{(u)}_c\left(b,\mu,\frac{\zeta_c}{\nu^2}\right) \equiv \sum_h \int_0^1 \mathrm{d}z\, z D^{(u)}_{1,h/c}\left(z,b,\mu,\frac{\zeta_c}{\nu^2}\right). \tag{39}$$

Similarly to the TMD PDFs, we define the "subtracted" TMD FFs in such a way that the standard soft function $\sqrt{S_{n_c\cdot\bar{n}_c}(b,L,L_\nu)}$ cancels out the rapidity divergence,

$$\begin{aligned} D_{1,h/c}(z,b,\mu,\zeta_c) = D^{(u)}_{1,h/c}&\left(z,b,\mu,\frac{\zeta_c}{\nu^2}\right) \\ &\times \sqrt{S_{n_c\cdot\bar{n}_c}(b,L,L_\nu)}. \end{aligned} \tag{40}$$

The evolution equation is given by,

$$\frac{\mathrm{d}}{\mathrm{d}\ln\mu} \ln D_{1,h/c}(z,b,\mu,\zeta_c) = \gamma^J_{\mu,c}\left[\alpha_s(\mu), \frac{\zeta_c}{\mu^2}\right], \tag{41}$$

where $\gamma^J_{\mu,c}[\alpha_s(\mu), \zeta_c/\mu^2]$ is the evolution kernel that governs the μ scale evolution of $D_{1,h/c}(z,b,\mu,\zeta_c)$ at fixed $\zeta = \zeta_c$. Up to two-loop order, $\gamma^J_{\mu,c}$ is given by,

$$\gamma^J_{\mu,c}\left[\alpha_s(\mu), \frac{\zeta_c}{\mu^2}\right] = -C_c \Gamma_{\mathrm{cusp}}[\alpha_s(\mu)] \ln\left(\frac{\zeta_c}{\mu^2}\right) + \gamma_c[\alpha_s(\mu)]. \tag{42}$$

The values of ζ_a, ζ_b and ζ_c can be found by demanding renormalization group (RG) consistency, i.e.,

$$\gamma^H_\mu + \gamma^f_{\mu,a} + \gamma^f_{\mu,b} + \gamma^S_\mu + \gamma^J_{\mu,c} = 0, \tag{43}$$

for both $q\bar{q} \to V + g$ and $qg \to V + q$ channels. We find that with the choice $\zeta_a = \zeta_b = \hat{s}$, and $\zeta_c = (\hat{s} - m_V^2)^2/\hat{s}$, the RG consistency is satisfied for both channels. Subsequently, the corresponding "subtracted" TEEC jet function $J_c(b, \mu, \zeta_c)$ can be written as,

$$J_c(b, \mu, \zeta_c) \equiv \sum_h \int_0^1 \mathrm{d}z\, z D_{1,h/c}(z, b, \mu, \zeta_c). \quad (44)$$

The TMD FFs $D_{1,h/c}(z, b, \mu, \zeta_c)$ with QCD evolution are given by,

$$\begin{aligned} D_{1,h/c}(z, b, \mu, \zeta_c) = \sum_i \int_z^1 \frac{\mathrm{d}y}{y} \hat{C}_{i\leftarrow c}\left(\frac{z}{y}, b\right) D_{h/i}(y, \mu_{b_*}) \\ \times \exp[-S_{\mathrm{pert}}(\mu, \mu_{b_*}, \zeta_c)] \\ \times \exp[-S^c_{\mathrm{NP}}(z, b, Q_0, \zeta_c)], \end{aligned} \quad (45)$$

where $Q_0^2 = 2.4\ \mathrm{GeV}^2$, $D_{h/i}$ are the vacuum collinear FFs and the matching coefficients $\hat{C}_{i\leftarrow c}$ can be found in [90,100–102]. The corresponding nonperturbative Sudakov factor $S^c_{\mathrm{NP}}(z, b, Q_0, \zeta_c)$ for quark and gluon are, respectively, given by [109]

$$S^q_{\mathrm{NP}}(z, b) = \frac{g_2}{2} \ln\left(\frac{b}{b_*}\right) \ln\left(\frac{\sqrt{\zeta_c}}{Q_0}\right) + g_1^D \frac{b^2}{z^2}, \quad (46)$$

$$S^g_{\mathrm{NP}}(z, b) = \frac{C_A}{C_F} \frac{g_2}{2} \ln\left(\frac{b}{b_*}\right) \ln\left(\frac{\sqrt{\zeta_c}}{Q_0}\right) + g_1^D \frac{b^2}{z^2}, \quad (47)$$

with $g_2 = 0.84$ and $g_1^D = 0.042\ \mathrm{GeV}^2$ [90,91] and we have omitted the Q_0 and ζ_c dependence for brevity.

Following the procedures in [52], we use the LO matching coefficients $\hat{C}_{i\leftarrow c}(z, b) = \delta_{ic}\delta(1 - z)$ in Eq. (45) and fit the z integration in Eq. (44) with [52,110],

$$\begin{aligned} \sum_h \int_0^1 \mathrm{d}z\, z D_{h/i}(z, \mu_{b_*}) \exp\left(-g_1^D \frac{b^2}{z^2}\right) \\ \equiv \exp[-S^{\mathrm{TEEC}}_{\mathrm{NP}}(b)], \end{aligned} \quad (48)$$

with the functional form,

$$S^{\mathrm{TEEC}}_{\mathrm{NP}}(b) = N b^\alpha (1 + r b^\beta). \quad (49)$$

Here N, α, r and β are the fit parameters and their extracted values are given in Table I. We emphasize that the conditions $\alpha > 0$ and $\beta > 0$ are imposed to guarantee that the second term ($N r b^{\alpha+\beta}$) maintains a strictly larger exponent than the first term ($N b^\alpha$). The parametrization chosen here is different from the previous choice made in [52], since the new parametrization is more flexible and can lead to a successful fit in both vacuum and nuclear environment. As for the choice of collinear FFs that enter Eq. (48), we use the 2021 DSS parametrization [111] for neutral and charged pions, i.e., π^0 and $\pi^\pm$. In order to remove the bias from including only pion FFs, we normalize the left-hand side of Eq. (48) by $\sum_{\pi^0,\pi^\pm} \int_0^1 \mathrm{d}z\, z D_{h/i}(z, \mu_{b_*})$. Note that in Eq. (49), the same set of parameters in $S^{\mathrm{TEEC}}_{\mathrm{NP}}(b)$ is used for quark and gluon since the sum rule $\sum_h \int_0^1 \mathrm{d}z\, z D_{h/i}(z, \mu_{b_*}) = 1$ holds for $i = q$ and g. Additionally, although the FFs for charged and neutral hadrons are currently available in vacuum [112], they have not been fitted in a nuclear environment yet. We therefore choose to use pion FFs in vacuum, so as to be consistent with the LIKEn pion FFs [113] we used in nuclear environment. We then have the final expressions for the quark and gluon TEEC jet functions,

TABLE I. Values of fitted parameters from Eq. (49). The values are approximated to the second digits after the decimal point. The average values and standard deviation for Au and Pb are calculated from 29 fits corresponding to the Hessian sets given in LIKEn 2021 FFs [113]. The r parameters for Au and Pb are displayed with three decimal places because their variations are smaller.

Nucleus	$N[\mathrm{GeV}^\alpha]$	α	$r[\mathrm{GeV}^\beta]$	β
p	0.45	0.42	0.63	1.00
Au	1.21 ± 0.02	0.56 ± 0.01	0.138 ± 0.008	1.21 ± 0.02
Pb	1.22 ± 0.03	0.56 ± 0.01	0.136 ± 0.007	1.22 ± 0.02

$$\begin{aligned} J_q(b, \mu, \zeta_c) = \exp[-S_{\mathrm{pert}}(\mu, \mu_{b_*}, \zeta_c)] \\ \times \exp\left[-\frac{g_2}{2} \ln\left(\frac{b}{b_*}\right) \ln\left(\frac{\sqrt{\zeta_c}}{Q_0}\right) - S^{\mathrm{TEEC}}_{\mathrm{NP}}(b)\right], \end{aligned} \quad (50)$$

$$\begin{aligned} J_g(b, \mu, \zeta_c) = \exp[-S_{\mathrm{pert}}(\mu, \mu_{b_*}, \zeta_c)] \\ \times \exp\left[-\frac{C_A}{C_F} \frac{g_2}{2} \ln\left(\frac{b}{b_*}\right) \ln\left(\frac{\sqrt{\zeta_c}}{Q_0}\right) - S^{\mathrm{TEEC}}_{\mathrm{NP}}(b)\right]. \end{aligned} \quad (51)$$

As one can expect from the TMD factorization formalism of TMD FFs, the quark and gluon TEEC jet functions are only different by a color factor C_A/C_F in the nonperturbative Sudakov factor.

The nuclear modification for TEEC jet function is considered following a procedure similar to the one for the TMD PDFs in Sec. II A. First we replace the vacuum collinear FFs $D_{h/i}$ in Eq. (45) with the nuclear FFs $D^A_{h/i}$. In this work, we use the LIKEn 2021 set [113] for both gold (Au) and lead (Pb). The fitted parameters are summarized in Table I. Additionally, we follow the work in [105] and introduce a new parameter $g^D_{1,A}$ in place of g^D_1 in Eqs. (46) and (47) such that,

$$g_{1,A}^D = g_1^D + b_N L, \tag{52}$$

where $L \equiv A^{1/3} - 1$ with A being the mass number of the nucleus, and $b_N = 0.0097\ \mathrm{GeV}^2$ has been determined from fitting experimental data [105]. See also Ref. [114].

An interesting point that we notice in Table I is that the fitted parameters for Au and Pb are very close to each other. This is due to the fact that the mass numbers of Au and Pb are very similar (197 and 208, respectively), and the only distinction in the parametrization of nuclear effects (in both collinear and TMD FFs) for Au and Pb lies in their mass numbers.

Finally, one can write the factorization formula in Eq. (3) using the "subtracted" TMD PDFs and TEEC jet functions as,

$$\frac{\mathrm{d}\Sigma}{\mathrm{d}\tau\,\mathrm{d}y_V\,\mathrm{d}p_{V,T}} = \sum_{a,b,c} \frac{p_{V,T}}{\sqrt{\tau}} \int_0^\infty \frac{\mathrm{d}b}{\pi} \cos(2b\sqrt{\tau}p_{V,T}) \int \mathrm{d}y_c H_{ab\to Vc}(y_V, p_{V,T}, m_V, \mu) \times x_a f_{1,a/p}(x_a, b, \mu, \zeta_a) x_b f_{1,b/p}(x_b, b, \mu, \zeta_b) J_c(b, \mu, \zeta_c) S^g_{abc}(b, \mu). \tag{53}$$

Following [105], we assume that the nuclear TMD factorization in pA collisions retains the same structure as the TMD factorization in pp collisions, except that the free TMD distributions (including both TMD PDFs and TMD FFs) are replaced by the nuclear TMD distributions discussed earlier. This assumption on nuclear TMD factorization has been examined in [105] using existing global data, including SIDIS in electron-nucleus collisions and DY dilepton production in proton-nucleus collisions. We believe that the future measurements of the TEEC observable, as presented in this work, will provide a valuable contribution to further validating the assumption.

In performing phenomenological studies, we choose to evolve the hard function, TMD PDFs, TEEC jet function as well as the soft function to a common scale $\mu = \sqrt{m_V^2 + p_{V,T}^2}$ with $m_V = 91.1876$ GeV for $Z + h$ and $m_V = 0$ GeV for $\gamma + h$. More details on the numerical values of relevant parameters will be discussed in Sec. III.

III. PHENOMENOLOGY

In this Section, we provide numerical predictions for the TEEC using the factorization formula in Eq. (53), both with the RHIC and LHC kinematics. Besides pp collisions, pAu collisions at RHIC and pPb collisions at LHC kinematics are also studied to assess nuclear TMD effects.

First, for the pp collisions at RHIC, we choose $\sqrt{s} = 200$ GeV, final-state photon $p_{V,T} \in (10, 20)$ GeV and rapidity range $y_V \in (-1, 1)$, $y_c \in (-1, 1)$. This corresponds to the kinematics and detector acceptance at sPHENIX experiment. The predictions for the TEEC in the process $pp \to \gamma + h$ at sPHENIX kinematics are shown in Fig. 2. The cross section decreases with increasing τ, which aligns with expectation, as the final-state photon and hadrons deviate further from the back-to-back configuration as τ becomes larger, resulting in a lower event count. In Fig. 2, we also present the uncertainty band, which is derived by varying μ around its nominal value, $\mu = \sqrt{m_V^2 + p_{V,T}^2}$, by factors of 0.5, 1, and 2, and then taking the envelope of the resulting variations.

In the upper panel of Fig. 3, we present the same observable in $pp \to \gamma + h$ at LHC energy. We use two rapidity ranges, one with $y_{V,c} \in (-2, 2)$ corresponding to the midrapidity, the other one with $y_{V,c} \in (2, 5)$ corresponding to the forward rapidity region. Finally in the lower panel of Fig. 3, we present the predicted $pp \to Z + h$ at LHC energy. A similar trend that was predicted for RHIC is observed here, which again agrees with our expectation. Additionally, the number of events at the forward rapidity bin are fewer than the one at the midrapidity bin, as expected. Again, the uncertainty bands in Fig. 3 reflect variations of μ around its nominal value by factors of 0.5, 1, and 2, with the envelope of the resulting variations defining the bands.

In order to study the nuclear effects, we present the result for pAu collision at sPHENIX at RHIC and pPb collision at LHC. First we define the nuclear modification factor as,

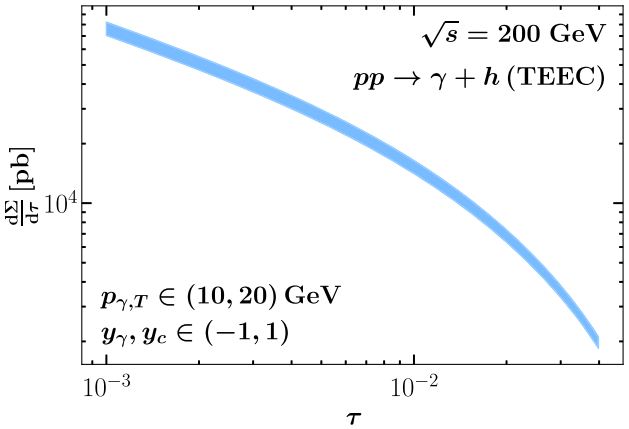


FIG. 2. Predictions for the TEEC observable in $pp \to \gamma + h$ at sPHENIX kinematics. Also shown in the figure are the kinematic requirements for photons. The uncertainty band reflects variations of μ around its nominal value by factors of 0.5, 1, and 2, and represents the envelope of the resulting variations.

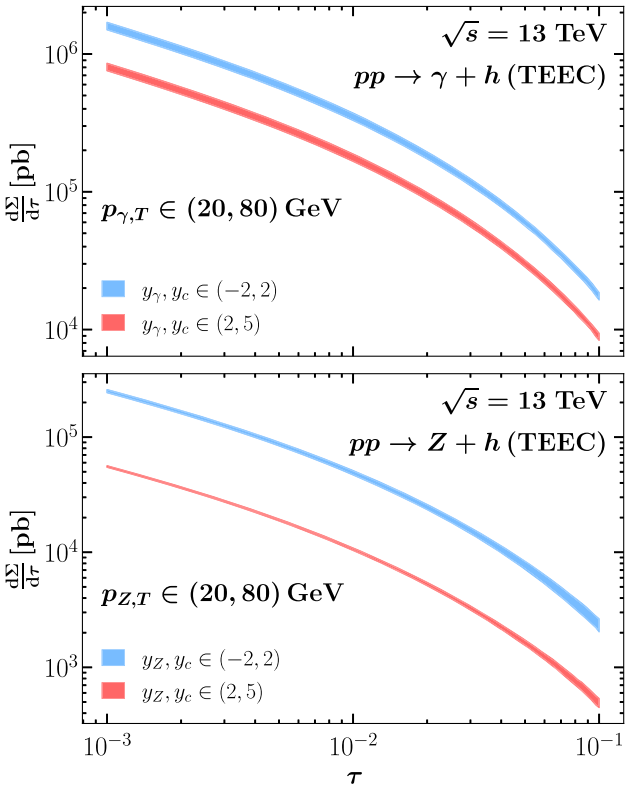


FIG. 3. Predictions for the TEEC observable at mid and forward rapidity. In the upper panel, the TEEC observables in $pp \to \gamma + h$ at mid (blue) and forward (red) rapidity regions are shown, while in the lower panel, the TEEC observables in $pp \to Z + h$ at mid (blue) and forward (red) rapidity regions are presented. The uncertainty bands reflect variations of μ around its nominal value by factors of 0.5, 1, and 2, with the envelope of these variations defining the bands.

$$R_{pA} \equiv \frac{1}{A} \frac{d\Sigma^{pA}}{d\tau\, dy_V\, dp_{V,T}} \Big/ \frac{d\Sigma^{pp}}{d\tau\, dy_V\, dp_{V,T}}, \tag{54}$$

where A in the subscript represents the nuclear target.

For pAu collision at RHIC, we plot the nuclear modification factor R_{pA} at $\sqrt{s} = 200$ GeV, with $p_T \in (10, 20)$ GeV and $y_\gamma, y_c \in (-1, 1)$. This is shown in Fig. 4. The band represents the uncertainties arising from variations in the choice of members from the nuclear collinear FFs [113]. At small τ, a nuclear modification of ~30% can be expected. On the other hand, the nuclear modification approaches or even exceeds 1 as τ gets larger. This is due to nuclear modification manifesting itself as a broadening effect in the transverse momentum distribution. To be more specific, larger τ values correspond to larger transverse momentum imbalance between the final-state boson and hadron, and since the transverse momentum gets smeared to larger values in the nuclear environment, the nuclear modification behaves as a suppression effect at smaller τ and enhancement at larger τ.

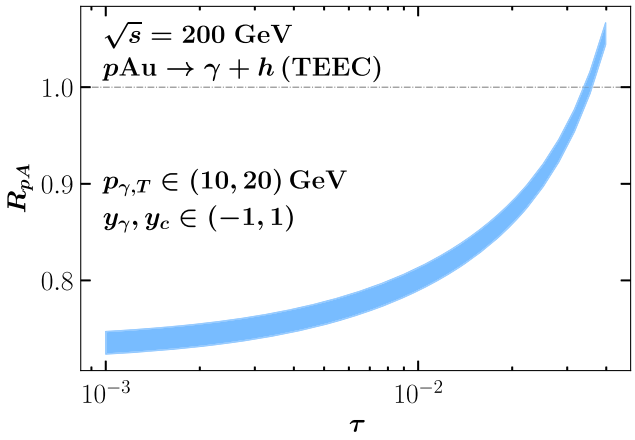


FIG. 4. Nuclear modification for pAu $\to \gamma + h$ at sPHENIX kinematics. The kinematics are labeled in the plots. The band represents the uncertainty from different members of nuclear collinear FFs [113].

We have also plotted the nuclear modification predictions for the LHC at mid and forward rapidity in Fig. 5. Similar behavior is observed between the RHIC and LHC

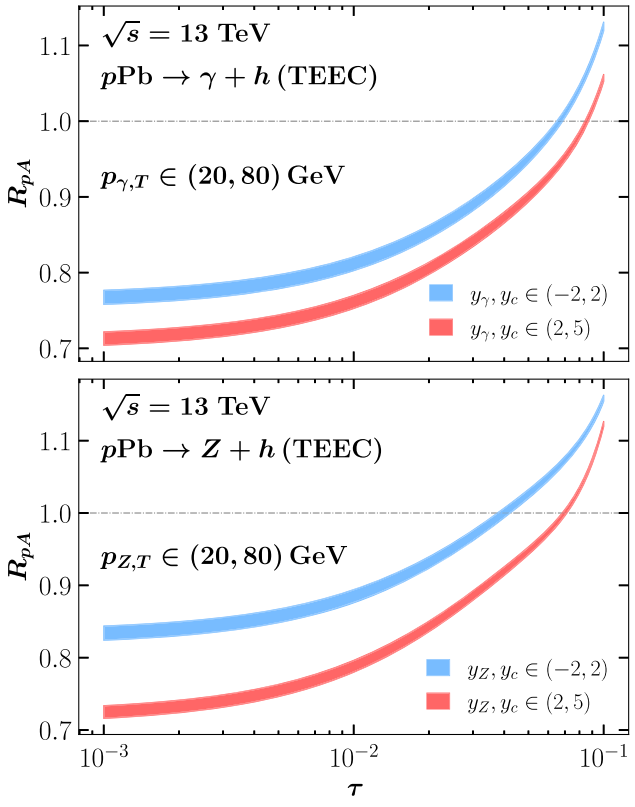


FIG. 5. In the upper panel, nuclear modifications for pPb $\to \gamma + h$ at mid (blue) and forward (blue) rapidity are shown. In the lower panel, nuclear modifications for pPb $\to Z + h$ at mid (blue) and forward (blue) rapidity regions are shown. The kinematic requirements are summarized in the figure. The bands represent the uncertainties arising from different choices of members from nuclear collinear FFs [113].

kinematics. Additionally, when comparing the R_{pA} in the central and forward regions, we find that the R_{pA} values are smaller in the forward rapidity region. This occurs because, in the forward rapidity region, the value of x_b [as given in Eq. (10)] becomes very small, entering deeper into the shadowing region of nuclear modification. This analysis highlights that the TEEC in pA collisions serves as an excellent observable for studying nuclear modification effects on TMDs. Specifically, the ability to measure a broad range of τ enables us to study the transverse momentum broadening in the nuclear medium, as encoded in the shape of the τ distribution. Furthermore, by examining the τ distribution across different rapidity regions, we can investigate nuclear modification in the collinear parton distribution functions.

IV. CONCLUSIONS

In this paper, we have explored the transverse energy-energy correlator in the pp collision for back-to-back γ-hadron and Z-hadron production at RHIC and the LHC. In the transverse plane, the azimuthal angle difference ϕ between the final-state vector boson and the hadron is measured, and we provide a factorization formula for this event-shape observable as $\phi \to \pi$. We present numerical results for TEEC in pp collisions, and find that the TEEC cross section decreases as τ gets larger.

Additionally, we study the nuclear modification in pAu collision at RHIC and pPb collision at LHC. We find that the nuclear modification factor can be $\sim$70% at low τ region and grows with τ. This observation agrees with our expectation that the nuclear medium broadens the transverse momentum distribution and thus smears the cross section to larger τ values, or equivalently gives rise to greater transverse momentum imbalance. Furthermore, we investigate the nuclear modification of the TEEC at both central and forward rapidity regions. Our findings indicate that measurements at different rapidities offer valuable insights into the nuclear modification of the collinear component of the TMD in nuclei. This highlights that the TEEC observable can serve as an effective probe for studying nuclear modification in TMD physics. Finally, the future measurement of the TEEC observables in proton-nucleus collisions could provide further validation of the assumptions made in the nuclear TMD factorization.

In summary, exploring the transverse energy-energy correlator in vector boson plus hadron production in proton-proton and proton-nucleus collisions presents a fertile ground for studying TMD physics, both in vacuum and nuclear environments. We anticipate the insights obtained from TEEC observables will be crucial in enhancing our understanding of the fundamental aspects of strong interaction physics. We encourage experiments at both RHIC and the LHC to carry out these measurements.

ACKNOWLEDGMENTS

Z. K. and J. P. are supported by the National Science Foundation under Grant No. PHY-1945471. S. L. is supported by U.S. Department of Energy under Contract No. DE-FG02-96ER40982. F. Z. is supported by U.S. Department of Energy, Office of Science, Office of Nuclear Physics under Contract No. DESC0011090 and U.S. Department of Energy, Office of Science, National Quantum Information Science Research Centers, Co-design Center for Quantum Advantage (C2QA) under Contract No. DESC0012704. Y. Z. is supported by the European Union "Next Generation EU" program through the Italian PRIN 2022 Grant No. 20225ZHA7W. Y. Z. is also supported by the Guangdong Major Project of Basic and Applied Basic Research No. 2020B0301030008, and the National Natural Science Foundation of China under Grants No. 12022512 and No. 12035007. This work is also supported by the U.S. Department of Energy, Office of Science, Office of Nuclear Physics, within the framework of the Saturated Glue (SURGE) Topical Theory Collaboration.

DATA AVAILABILITY

No data were created or analyzed in this study.

[1] R. Abbate, M. Fickinger, A. Hoang, V. Mateu, and I. W. Stewart, Global fit of $\alpha_s(M_Z)$ to thrust at N^{3}LL order with power corrections, Proc. Sci., RADCOR2009 (**2010**) 040 [arXiv:1004.4894].

[2] A. H. Hoang, D. W. Kolodrubetz, V. Mateu, and I. W. Stewart, Precise determination of α_s from the C-parameter distribution, Phys. Rev. D **91**, 094018 (2015).

[3] V. Andreev *et al.* (H1 Collaboration), Determination of the strong coupling constant $\alpha_s(m_Z)$ in next-to-next-to-leading order QCD using H1 jet cross section measurements, Eur. Phys. J. C **77**, 791 (2017); **81**, 738(E) (2021).

[4] A. Banfi, G. P. Salam, and G. Zanderighi, Phenomenology of event shapes at hadron colliders, J. High Energy Phys. 06 (2010) 038.

[5] V. Khachatryan *et al.* (CMS Collaboration), First measurement of hadronic event shapes in pp collisions at $\sqrt{s} = 7$ TeV, Phys. Lett. B **699**, 48 (2011).

[6] G. Aad *et al.* (ATLAS Collaboration), Measurement of event shapes at large momentum transfer with the ATLAS detector in pp collisions at $\sqrt{s} = 7$ TeV, Eur. Phys. J. C **72**, 2211 (2012).

[7] S. Chatrchyan *et al.* (CMS Collaboration), Event shapes and azimuthal correlations in $Z +$ jets events in pp collisions at $\sqrt{s} = 7$ TeV, Phys. Lett. B **722**, 238 (2013).

[8] V. Khachatryan *et al.* (CMS Collaboration), Study of hadronic event-shape variables in multijet final states in pp collisions at $\sqrt{s} = 7$ TeV, J. High Energy Phys. 10 (2014) 087.

[9] G. Aad *et al.* (ATLAS Collaboration), Measurement of transverse energy-energy correlations in multi-jet events in pp collisions at $\sqrt{s} = 7$ TeV using the ATLAS detector and determination of the strong coupling constant $\alpha_s(m_Z)$, Phys. Lett. B **750**, 427 (2015).

[10] M. Aaboud *et al.* (ATLAS Collaboration), Determination of the strong coupling constant α_s from transverse energy–energy correlations in multijet events at $\sqrt{s} = 8$ TeV using the ATLAS detector, Eur. Phys. J. C **77**, 872 (2017).

[11] A. M. Sirunyan *et al.* (CMS Collaboration), Event shape variables measured using multijet final states in proton-proton collisions at $\sqrt{s} = 13$ TeV, J. High Energy Phys. 12 (2018) 117.

[12] G. Aad *et al.* (ATLAS Collaboration), Determination of the strong coupling constant from transverse energy–energy correlations in multijet events at $\sqrt{s} = 13$ TeV with the ATLAS detector, J. High Energy Phys. 07 (2023) 085.

[13] M. Czakon, A. Mitov, and R. Poncelet, Next-to-next-to-leading order study of three-jet production at the LHC, Phys. Rev. Lett. **127**, 152001 (2021); **129**, 119901(E) (2022).

[14] M. Alvarez, J. Cantero, M. Czakon, J. Llorente, A. Mitov, and R. Poncelet, NNLO QCD corrections to event shapes at the LHC, J. High Energy Phys. 03 (2023) 129.

[15] G. Aad *et al.* (ATLAS Collaboration), Measurement of charged-particle event shape variables in $\sqrt{s} = 7$ TeV proton-proton interactions with the ATLAS detector, Phys. Rev. D **88**, 032004 (2013).

[16] G. Aad *et al.* (ATLAS Collaboration), Properties of jet fragmentation using charged particles measured with the ATLAS detector in pp collisions at $\sqrt{s} = 13$ TeV, Phys. Rev. D **100**, 052011 (2019).

[17] S. Acharya *et al.* (ALICE Collaboration), Exploration of jet substructure using iterative declustering in pp and Pb − Pb collisions at LHC energies, Phys. Lett. B **802**, 135227 (2020).

[18] S. Acharya *et al.* (ALICE Collaboration), Measurements of the groomed and ungroomed jet angularities in pp collisions at $\sqrt{s} = 5.02$ TeV, J. High Energy Phys. 05 (2022) 061.

[19] S. Acharya *et al.* (ALICE Collaboration), First measurements of N-subjettiness in central Pb − Pb collisions at $\sqrt{s_{\mathrm{NN}}} = 2.76$ TeV, J. High Energy Phys. 10 (2021) 003.

[20] D. Kang, C. Lee, and I. W. Stewart, Using 1-jettiness to measure 2 jets in DIS 3 Ways, Phys. Rev. D **88**, 054004 (2013).

[21] Z.-B. Kang, X. Liu, and S. Mantry, 1-jettiness DIS event shape: NNLL + NLO results, Phys. Rev. D **90**, 014041 (2014).

[22] H. Cao, Z.-B. Kang, X. Liu, and S. Mantry, One-jettiness DIS event shape at N3LL + O(αs2), Phys. Rev. D **110**, 014045 (2024).

[23] V. Andreev *et al.* (H1 Collaboration), Measurement of the 1-jettiness event shape observable in deep-inelastic electron-proton scattering at HERA, Eur. Phys. J. C **84**, 785 (2024).

[24] V. Andreev *et al.* (H1 Collaboration), Measurement of groomed event shape observables in deep-inelastic electron-proton scattering at HERA, Eur. Phys. J. C **84**, 718 (2024).

[25] D. Boer *et al.*, Gluons and the quark sea at high energies: Distributions, polarization, tomography, arXiv:1108.1713.

[26] A. Accardi *et al.*, Electron ion collider: The next QCD frontier: Understanding the glue that binds us all, Eur. Phys. J. A **52**, 268 (2016).

[27] R. Abdul Khalek *et al.*, Science requirements and detector concepts for the electron-ion collider: EIC Yellow report, Nucl. Phys. **A1026**, 122447 (2022).

[28] R. Abdul Khalek *et al.*, Snowmass 2021 white paper: Electron ion collider for high energy physics, arXiv: 2203.13199.

[29] D. E. Kaplan and M. D. Schwartz, Constraining light colored particles with event shapes, Phys. Rev. Lett. **101**, 022002 (2008).

[30] J. Llorente and B. P. Nachman, Limits on new coloured fermions using precision jet data from the large hadron collider, Nucl. Phys. **B936**, 106 (2018).

[31] A. Ali, E. Pietarinen, and W. J. Stirling, Transverse energy-energy correlations: A test of perturbative QCD for the proton—anti-proton collider, Phys. Lett. **141B**, 447 (1984).

[32] C. L. Basham, L. S. Brown, S. D. Ellis, and S. T. Love, Energy correlations in electron-positron annihilation: Testing QCD, Phys. Rev. Lett. **41**, 1585 (1978).

[33] C. L. Basham, L. S. Brown, S. D. Ellis, and S. T. Love, Energy correlations in electron-positron annihilation in quantum chromodynamics: Asymptotically free perturbation theory, Phys. Rev. D **19**, 2018 (1979).

[34] K. Abe *et al.* (SLD Collaboration), Measurement of $\alpha_s(m_Z^2)$ from hadronic event observables at the Z^0 resonance, Phys. Rev. D **51**, 962 (1995).

[35] O. Adrian *et al.* (L3 Collaboration), Determination of α_s from hadronic event shapes measured on the Z^0 resonance, Phys. Lett. B **284**, 471 (1992).

[36] P. D. Acton *et al.* (OPAL Collaboration), An improved measurement of $\alpha_s(m_{Z^0})$ using energy correlations with the OPAL detector at LEP, Phys. Lett. B **276**, 547 (1992).

[37] I. Adachi *et al.* (TOPAZ Collaboration), Measurements of α_s in e^+e^- annihilation at $\sqrt{s} = 53.3$ GeV and 59.5-GeV, Phys. Lett. B **227**, 495 (1989).

[38] W. Braunschweig *et al.* (TASSO Collaboration), A study of energy-energy correlations Between 12-GeV and 46.8-GeV CM energies, Z. Phys. C **36**, 349 (1987).

[39] W. Bartel *et al.* (JADE Collaboration), Measurements of energy correlations in $e^+e^- \to$ hadrons, Z. Phys. C **25**, 231 (1984).

[40] E. Fernandez *et al.*, A measurement of energy-energy correlations in $e^+e^- \to$ hadrons at $\sqrt{s} = 29$ GeV, Phys. Rev. D **31**, 2724 (1985).

[41] D. R. Wood *et al.*, Determination of α_s from energy-energy correlations in e^+e^- annihilation at 29 GeV, Phys. Rev. D **37**, 3091 (1988).

[42] H. J. Behrend *et al.* (CELLO Collaboration), Analysis of the energy weighted angular correlations in hadronic e^+e^- annihilations at 22 GeV and 34 GeV, Z. Phys. C **14**, 95 (1982).

[43] C. Berger *et al.* (PLUTO Collaboration), A study of energy-energy correlations in e^+e^- annihilations at $\sqrt{s} = 34.6$-GeV, Z. Phys. C **28**, 365 (1985).

[44] M. Z. Akrawy *et al.* (OPAL Collaboration), A measurement of energy correlations and a determination of $\alpha_s(M^2_{Z^0})$ in e^+e^- annihilations at $\sqrt{s} = 91$ GeV, Phys. Lett. B **252**, 159 (1990).

[45] D. Decamp *et al.* (ALEPH Collaboration), Measurement of α_s from the structure of particle clusters produced in hadronic Z decays, Phys. Lett. B **257**, 479 (1991).

[46] B. Adeva *et al.* (L3 Collaboration), Determination of α_s from energy-energy correlations measured on the Z^0 resonance., Phys. Lett. B **257**, 469 (1991).

[47] K. Abe *et al.* (SLD Collaboration), Measurement of α_s from energy-energy correlations at the Z^0 resonance, Phys. Rev. D **50**, 5580 (1994).

[48] ATLAS Collaboration, Determination of the strong coupling constant and test of asymptotic freedom from transverse energy-energy correlations in multijet events at $\sqrt{s} = 13$ TeV with the ATLAS detector Report No. ATLAS-CONF-2020-025, 2020, https://inspirehep.net/literature/1809628.

[49] A. Ali, F. Barreiro, J. Llorente, and W. Wang, Transverse energy-energy correlations in next-to-leading order in α_s at the LHC, Phys. Rev. D **86**, 114017 (2012).

[50] A. Gao, H. T. Li, I. Moult, and H. X. Zhu, Precision QCD event shapes at hadron colliders: The transverse energy-energy correlator in the back-to-back limit, Phys. Rev. Lett. **123**, 062001 (2019).

[51] H. T. Li, I. Vitev, and Y. J. Zhu, Transverse-energy-energy correlations in deep inelastic scattering, J. High Energy Phys. 11 (2020) 051.

[52] Z.-B. Kang, J. Penttala, F. Zhao, and Y. Zhou, Transverse energy-energy correlators in the color-glass condensate at the electron-ion collider, Phys. Rev. D **109**, 094012 (2024).

[53] A. Hayrapetyan *et al.* (CMS Collaboration), Measurement of energy correlators inside jets and determination of the strong coupling $\alpha_S(m_Z)$, Phys. Rev. Lett. **133**, 071903 (2024).

[54] S. Acharya *et al.* (ALICE Collaboration), Exposing the parton-hadron transition within jets with energy-energy correlators in pp collisions at $\sqrt{s} = 5.02$ TeV, arXiv:2409.12687.

[55] A. Gao, J. K. L. Michel, I. W. Stewart, and Z. Sun, Better angle on hadron transverse momentum distributions at the electron-ion collider, Phys. Rev. D **107**, L091504 (2023).

[56] Z.-B. Kang, K. Lee, D. Y. Shao, and F. Zhao, Probing transverse momentum dependent structures with azimuthal dependence of energy correlators, J. High Energy Phys. 03 (2024) 153.

[57] M. Aaboud *et al.* (ATLAS Collaboration), Comparison of fragmentation functions for jets dominated by light quarks and gluons from pp and Pb + Pb collisions in ATLAS, Phys. Rev. Lett. **123**, 042001 (2019).

[58] R. Aaij *et al.* (LHCb Collaboration), Measurement of charged hadron production in Z-tagged jets in proton-proton collisions at $\sqrt{s} = 8$ TeV, Phys. Rev. Lett. **123**, 232001 (2019).

[59] A. Tumasyan *et al.* (CMS Collaboration), Study of quark and gluon jet substructure in Z + jet and dijet events from pp collisions, J. High Energy Phys. 01 (2022) 188.

[60] LHCb Collaboration, Multidifferential study of identified charged hadron distributions in Z-tagged jets in proton-proton collisions at $\sqrt{s} = 13$ TeV, Phys. Rev. D **108**, L031103 (2023).

[61] A. Gao, H. T. Li, I. Moult, and H. X. Zhu, The transverse energy-energy correlator at next-to-next-to-next-to-leading logarithm, J. High Energy Phys. 09 (2024) 072.

[62] V. Kartvelishvili, R. Kvatadze, and R. Shanidze, On Z and Z + jet production in heavy ion collisions, Phys. Lett. B **356**, 589 (1995).

[63] X.-N. Wang and Z. Huang, Study medium induced parton energy loss in γ + jet events of high-energy heavy ion collisions, Phys. Rev. C **55**, 3047 (1997).

[64] X.-N. Wang, Z. Huang, and I. Sarcevic, Jet quenching in the opposite direction of a tagged photon in high-energy heavy ion collisions, Phys. Rev. Lett. **77**, 231 (1996).

[65] X.-N. Wang and Y. Zhu, Medium modification of γ-jets in high-energy heavy-ion collisions, Phys. Rev. Lett. **111**, 062301 (2013).

[66] W. Dai, I. Vitev, and B.-W. Zhang, Momentum imbalance of isolated photon-tagged jet production at RHIC and LHC, Phys. Rev. Lett. **110**, 142001 (2013).

[67] Z.-B. Kang, I. Vitev, and H. Xing, Vector-boson-tagged jet production in heavy ion collisions at energies available at the CERN Large Hadron Collider, Phys. Rev. C **96**, 014912 (2017).

[68] G.-Y. Qin, J. Ruppert, C. Gale, S. Jeon, and G. D. Moore, Jet energy loss, photon production, and photon-hadron correlations at RHIC, Phys. Rev. C **80**, 054909 (2009).

[69] M. Aaboud *et al.* (ATLAS Collaboration), Measurement of jet p_{T} correlations in Pb + Pb and pp collisions at $\sqrt{s_{\mathrm{NN}}} = 2.76$ TeV with the ATLAS detector, Phys. Lett. B **774**, 379 (2017).

[70] S. Chatrchyan *et al.* (CMS Collaboration), Jet momentum dependence of jet quenching in PbPb collisions at $\sqrt{s_{NN}} = 2.76$ TeV, Phys. Lett. B **712**, 176 (2012).

[71] M. Aaboud *et al.* (ATLAS Collaboration), Measurement of photon–jet transverse momentum correlations in 5.02 TeV Pb + Pb and pp collisions with ATLAS, Phys. Lett. B **789**, 167 (2019).

[72] A. M. Sirunyan *et al.* (CMS Collaboration), Study of jet quenching with isolated-photon + jet correlations in PbPb and pp collisions at $\sqrt{s_{\mathrm{NN}}} = 5.02$ TeV, Phys. Lett. B **785**, 14 (2018).

[73] M. Aaboud *et al.* (ATLAS Collaboration), Measurement of jet fragmentation in Pb + Pb and pp collisions at $\sqrt{s_{NN}} = 5.02$ TeV with the ATLAS detector, Phys. Rev. C **98**, 024908 (2018).

[74] S. Chatrchyan *et al.* (CMS Collaboration), Measurement of Jet Fragmentation in PbPb and pp Collisions at $\sqrt{s_{NN}} = 2.76$ TeV, Phys. Rev. C **90**, 024908 (2014).

[75] S. Fang, W. Ke, D. Y. Shao, and J. Terry, Precision three-dimensional imaging of nuclei using recoil-free jets, J. High Energy Phys. 05 (2024) 066.
[76] M.-S. Gao, Z.-B. Kang, D. Y. Shao, J. Terry, and C. Zhang, QCD resummation of dijet azimuthal decorrelations in pp and pA collisions, J. High Energy Phys. 10 (2023) 013.
[77] R. Boussarie *et al.*, TMD handbook, arXiv:2304.03302.
[78] J.-Y. Chiu, A. Jain, D. Neill, and I. Z. Rothstein, A formalism for the systematic treatment of rapidity logarithms in quantum field theory, J. High Energy Phys. 05 (2012) 084.
[79] Y.-T. Chien, D. Y. Shao, and B. Wu, Resummation of boson-jet correlation at hadron colliders, J. High Energy Phys. 11 (2019) 025.
[80] Y.-T. Chien, R. Rahn, D. Y. Shao, W. J. Waalewijn, and B. Wu, Precision boson-jet azimuthal decorrelation at hadron colliders, J. High Energy Phys. 02 (2023) 256.
[81] T. Becher and M. D. Schwartz, Direct photon production with effective field theory, J. High Energy Phys. 02 (2010) 040.
[82] G. P. Korchemsky and A. V. Radyushkin, Renormalization of the Wilson loops beyond the leading order, Nucl. Phys. **B283**, 342 (1987).
[83] T. Becher, M. Neubert, and B. D. Pecjak, Factorization and momentum-space resummation in deep-inelastic scattering, J. High Energy Phys. 01 (2007) 076.
[84] A. Jain, M. Procura, and W. J. Waalewijn, Parton fragmentation within an identified Jet at NNLL, J. High Energy Phys. 05 (2011) 035.
[85] J. Collins, *Foundations of Perturbative QCD*, Vol. 32 of Cambridge Monographs on Particle Physics, Nuclear Physics and Cosmology (Cambridge University Press, Cambridge, England, 2023).
[86] M. A. Ebert, I. W. Stewart, and Y. Zhao, Towards quasi-transverse momentum dependent PDFs computable on the lattice, J. High Energy Phys. 09 (2019) 037.
[87] Z.-B. Kang, K. Lee, D. Y. Shao, and F. Zhao, Spin asymmetries in electron-jet production at the future electron ion collider, J. High Energy Phys. 11 (2021) 005.
[88] I. Moult, H. X. Zhu, and Y. J. Zhu, The four loop QCD rapidity anomalous dimension, J. High Energy Phys. 08 (2022) 280.
[89] C. Duhr, B. Mistlberger, and G. Vita, Four-loop rapidity anomalous dimension and event shapes to fourth logarithmic order, Phys. Rev. Lett. **129**, 162001 (2022).
[90] M. G. Echevarria, Z.-B. Kang, and J. Terry, Global analysis of the Sivers functions at NLO + NNLL in QCD, J. High Energy Phys. 01 (2021) 126.
[91] P. Sun, J. Isaacson, C. P. Yuan, and F. Yuan, Nonperturbative functions for SIDIS and Drell–Yan processes, Int. J. Mod. Phys. A **33**, 1841006 (2018).
[92] J. Isaacson, Y. Fu, and C. P. Yuan, Improving ResBos for the precision needs of the LHC, Phys. Rev. D **110**, 073002 (2024).
[93] J. C. Collins, D. E. Soper, and G. F. Sterman, Transverse momentum distribution in Drell-Yan pair and W and Z boson production, Nucl. Phys. **B250**, 199 (1985).
[94] C. Balazs, E. L. Berger, S. Mrenna, and C. P. Yuan, Photon pair production with soft gluon resummation in hadronic interactions, Phys. Rev. D **57**, 6934 (1998).
[95] C. Balazs and C. P. Yuan, Higgs boson production at the LHC with soft gluon effects, Phys. Lett. B **478**, 192 (2000).
[96] C. Balazs, E. L. Berger, P. M. Nadolsky, and C. P. Yuan, Calculation of prompt diphoton production cross-sections at Tevatron and LHC energies, Phys. Rev. D **76**, 013009 (2007).
[97] S. M. Aybat and T. C. Rogers, TMD parton distribution and fragmentation functions with QCD evolution, Phys. Rev. D **83**, 114042 (2011).
[98] Z.-B. Kang, A. Prokudin, P. Sun, and F. Yuan, Extraction of quark transversity distribution and collins fragmentation functions with QCD evolution, Phys. Rev. D **93**, 014009 (2016).
[99] M. G. Echevarria, I. Scimemi, and A. Vladimirov, Unpolarized transverse momentum dependent parton distribution and fragmentation functions at next-to-next-to-leading order, J. High Energy Phys. 09 (2016) 004.
[100] M.-x. Luo, T.-Z. Yang, H. X. Zhu, and Y. J. Zhu, Quark transverse parton distribution at the next-to-next-to-next-to-leading order, Phys. Rev. Lett. **124**, 092001 (2020).
[101] M.-x. Luo, T.-Z. Yang, H. X. Zhu, and Y. J. Zhu, Unpolarized quark and gluon TMD PDFs and FFs at N^3LO, J. High Energy Phys. 06 (2021) 115.
[102] M. A. Ebert, B. Mistlberger, and G. Vita, Transverse momentum dependent PDFs at N^3LO, J. High Energy Phys. 09 (2020) 146.
[103] K. J. Eskola, P. Paakkinen, H. Paukkunen, and C. A. Salgado, EPPS16: Nuclear parton distributions with LHC data, Eur. Phys. J. C **77**, 163 (2017).
[104] S. Dulat, T.-J. Hou, J. Gao, M. Guzzi, J. Huston, P. Nadolsky, J. Pumplin, C. Schmidt, D. Stump, and C. P. Yuan, New parton distribution functions from a global analysis of quantum chromodynamics, Phys. Rev. D **93**, 033006 (2016).
[105] M. Alrashed, D. Anderle, Z.-B. Kang, J. Terry, and H. Xing, Three-dimensional imaging in nuclei, Phys. Rev. Lett. **129**, 242001 (2022).
[106] J.-y. Chiu, A. Jain, D. Neill, and I. Z. Rothstein, The rapidity renormalization group, Phys. Rev. Lett. **108**, 151601 (2012).
[107] M. G. A. Buffing, Z.-B. Kang, K. Lee, and X. Liu, A transverse momentum dependent framework for back-to-back photon + jet production, arXiv:1812.07549.
[108] I. Moult and H. X. Zhu, Simplicity from Recoil: The three-loop soft function and factorization for the energy-energy correlation, J. High Energy Phys. 08 (2018) 160.
[109] Z.-B. Kang, X. Liu, F. Ringer, and H. Xing, The transverse momentum distribution of hadrons within jets, J. High Energy Phys. 11 (2017) 068.
[110] H. T. Li, Y. Makris, and I. Vitev, Energy-energy correlators in deep inelastic scattering, Phys. Rev. D **103**, 094005 (2021).
[111] I. Borsa, D. de Florian, R. Sassot, and M. Stratmann, Pion fragmentation functions at high energy colliders, Phys. Rev. D **105**, L031502 (2022).
[112] I. Borsa, M. Stratmann, D. de Florian, and R. Sassot, Charged hadron fragmentation functions at high energy colliders, Phys. Rev. D **109**, 052004 (2024).
[113] P. Zurita, Medium modified fragmentation functions with open source xFitter, arXiv:2101.01088.
[114] M. Alrashed, Z.-B. Kang, J. Terry, H. Xing, and C. Zhang, Nuclear modified transverse momentum dependent parton distribution and fragmentation functions, arXiv:2312.09226.